IEEE Access
Multidisciplinary ⋮ Rapid Review ⋮ Open Access Journal

Received June 10, 2021, accepted July 4, 2021, date of publication July 12, 2021, date of current version July 20, 2021.

Digital Object Identifier 10.1109/ACCESS.2021.3096201

Blind Correction of Lateral Chromatic Aberration in Raw Bayer Data

STEFAN PETERSSON[1], HÅKAN GRAHN[1], AND JIM RASMUSSON[2]
[1]Department of Computer Science, Blekinge Institute of Technology, 371 79 Karlskrona, Sweden
[2]Sony Mobile Communications AB, 221 88 Lund, Sweden

Corresponding author: Stefan Petersson (stefan.petersson@bth.se)

This work was supported in part by the Knowledge Foundation in Sweden through the Scalable Resource-Efficient Systems for Big Data Analytics under Grant 20140032.

ABSTRACT Chromatic aberration is an error that occurs in color images due to the fact that camera lenses refract the light of different wavelengths in different angles. The common approach today to correct the error is to use a lookup table for each camera-lens combination, e.g., as in Adobe PhotoShop Lightroom or DxO Optics Pro. In this paper, we propose a method that corrects the chromatic aberration error without any priot knowledge of the camera-lens combination, and does the correction already on the bayer data, i.e., before the Raw image data is interpolated to an RGB image. We evaluate our method in comparison to DxO Optics Pro, a state-of-the-art tool based on lookup tables, using 25 test images and the variance of the color differences (VCD) metric. The results show that our blind method has a similar error correction performance as DxO Optics Pro, but without prior knowledge of the camera-lens setup.

INDEX TERMS Chromatic aberration, structural instability, image enhancement, blind correction, GPGPU.

I. INTRODUCTION

Color images acquired through different types of imaging optics are commonly distorted by various types of optical aberrations. One of the resulting errors is denoted as chromatic aberration (CA). Chromatic aberration occurs because lenses, typically made of glass or plastic, have different material dispersions and light of different wavelengths therefore refract at different angles. The main consequence in imaging is that light rays of different wavelengths are focused at different image distances (axial/longitudinal CA) and at different locations in the image (transverse/lateral CA), as shown in Figure 1.

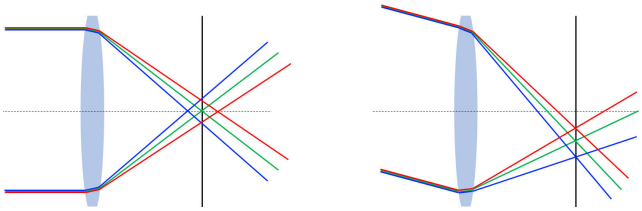

FIGURE 1. Illustration of axial (or longitudinal) chromatic aberration (ACA), to the left, and lateral (or transverse) chromatic aberration (LCA), to the right.

A digital color image is normally made up of three color channels. Lateral CA causes the color channels to be misaligned with respect to each other, which shows up as color fringes around edges and high contrast areas in the color image, as shown in Figure 2(b). The red and blue colors of different wavelengths are not focused at the same point as the green color. For example, this is clearly observed in Figure 2(b) as a red fringe along the edge of the light object.

In the manufacturing process of camera lenses, various lenses are combined to correct, or at least reduce, the chromatic aberration. However, even if several lenses are combined, it is non-trivial to completely align the three color channels to avoid chromatic aberration. Also, cameras in mobile phones or tablets are typically equipped with very compact and small lenses, which are prone to result in more CA. Image pixel resolution increases in a rapid pace, which is another high-impact factor since the CA pixel area will cover a larger number of pixels.

These types of imaging artifacts are unacceptable in professional photography. Software programs that correct imaging artifacts by post-processing of digital color images are readily available, including Adobe PhotoShop Lightroom CC®, Adobe Camera Raw®, DxO Optics Pro®, and PTLens®.

The associate editor coordinating the review of this manuscript and approving it for publication was Gulistan Raja.

(a) Full image (b) Uncorrected (c) Corrected

FIGURE 2. Visual comparison where lateral chromatic aberration is uncorrected (b), and corrected using our proposed method (c).

These software programs apply so-called *non-blind corrections*, i.e., they use *pre-calibrated correction parameters* for the specific combination of camera and lens that was used to capture the image to be corrected. Non-blind correction techniques must have access to a huge database of correction parameters for all possible combinations of cameras and lenses. Such a database takes a lot of effort to generate and must be constantly updated to account for new models of cameras and lenses, and combinations thereof.

As a result of the above, there is a strong need for *blind correction techniques* that are capable of correcting chromatic aberration in color images, including lateral CA, *without prior knowledge* about the color image and how it was generated (e.g., specific camera/lens combinations). Software programs for blind correction of lateral CA are known in previous work, e.g. RawTherapee. There is a general desire to provide alternative techniques for blind correction of lateral CA, especially a technique that is computationally efficient and capable of providing a significant reduction of lateral CA in a digital color image.

Previous work, e.g., by Wang *et al.* [1], have shown that it is important to correct CA before any demosaicing takes place, i.e., the processing step where the Bayer CFA (color filter array) information is interpolated to an RGB image. They have shown that CA correction has a positive effect on the demosaicing quality if it is done before the demosaicing step. Imatest goes one step further and claims that ''lateral CA cannot be reliably corrected after demosaicing, but it can be corrected to near-perfection prior to demosaicing'' [2].

In this paper, we propose a *novel blind method to correct lateral chromatic aberration* before any Bayer CFA to RGB interpolation (demosaicing) takes place. Most auto-focus cameras focus on the green channel when images are captured and our method assumes that the processed image data was taken using a camera with such logic. The main reason for this is that the Bayer color filter array contains twice as many green pixels as red and blue pixels, and therefore we assume that the green color channel is most correct one. The proposed method aligns and re-samples the red and blue channels so they match the green channel, similarly to for example [3]–[5]. The green channel is assumed to be correct already, and is therefore not modified in any way.

The proposed method is evaluated using 25 images in RAW format and of different sizes. Each image is CA corrected using our proposed method and compared to an image corrected with the DxO Optics Pro software. As evaluation metric, we use variance of color differences (VCD), which is used to evaluate CA artefacts [5], [6]. Our results show that, on average, the proposed method results in fewer CA artifacts as compared to the images corrected with DxO Optics Pro.

Our main contributions are:

- A novel method for blind correction of lateral chromatic aberration, i.e., without any lookup tables or prior knowledge of the camera / lens combination.
- Our proposed method uses raw camera image data as input, in order to have as good and undistorted data as possible.
- A highly efficient parallel GPU implementation of the method.
- An experimental evaluation showing results on par with state-of-the-art non-blind techniques, such as DxO Optics Pro.

The rest of the paper is organized as follows. In Section II, we present some background information and high-light related work. Then, we present our proposed method in Section III. In Section IV we present our evaluation methodology, while our experimental results and analysis are presented in Section V. Finally, we conclude our study in Section VI.

II. BACKGROUND AND RELATED WORK

A. DEMOSAICING

Most digital cameras acquire color data using a single charge-coupled device (CCD) sensor. This solution is very limiting, since only one third of the scene color information is stored for later interpretation. A color filter array (CFA) is placed in front of the sensor to capture one color component per pixel. The missing two color components are later interpolated for each pixel in the demosaicing process. The most common CFA pattern is the Bayer pattern [7], as shown in Figure 3.

The demosaicing process is central in the camera pipeline and has a major impact on the final image quality. Demosaicing techniques have different qualities, e.g., in terms of

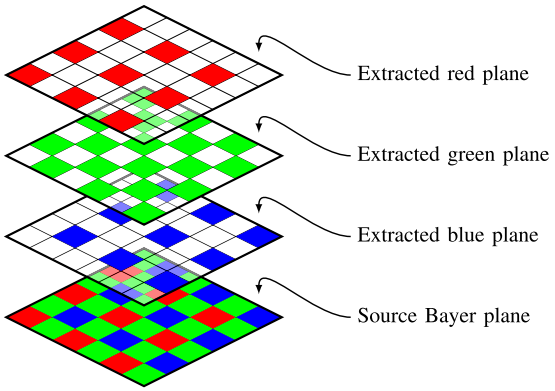

FIGURE 3. Separation of RGB planes from a Bayer plane.

interpolation quality and computational complexity. High interpolation quality often requires a high complexity technique. It is common to demosaic in either the spatial domain [8]–[11] or the frequency domain [12], [13] using single or multi-pass interpolation strategies.

Modern demosaicing methods take advantage of the correlation between color channels. The interpolation process may break down, introducing, e.g., false colors, more zippering artifacts, etc., in areas where the chromatic aberration is severe. The CA correction analysis relies on true edge information, i.e, lines where some of the color planes change intensity drastically. Since the resulting RGB data may contain multiple interpolation errors, it is non-trivial to determine what image regions to analyze further.

B. CHROMATIC ABERRATION

Chromatic aberration (CA) is a problem that is present in all images, and arises when light passes through a lens. Since the light consists of colors of different wavelengths, different colors will then be refracted at different angels when passing through a lens. As a result, color fringes may show up at object edges and in high-contrast areas, as shown in Figure 2(b).

Chromatic aberration can be divided into two different types: axial (or longitudinal) chromatic aberration (ACA), and lateral (or transverse) chromatic aberration (LCA), as shown in Figure 1. Axial CA are shifts along the optical axis while lateral CA are shifts perpendicular to the optical axis. Our proposed approach corrects *lateral CA* by realigning color planes from the color filter array. Our proposed approach realign the red and blue color planes before demosaicing takes place, as motivated in [1], since after demosaicing the color channels are interpolated and possibly disturbed.

C. RELATED WORK

Kühn *et al.* [14] presented some early work on how to spatially align two colors with different wavelengths in real-time. Their context was digital holographic microscopy, where a single holographic image is acquired. The idea is based on two reference waves that are aligned and centered in the Fourier plane, and then are transferred back using an inverse Fourier transform.

Kang [15] presents a technique to reduce the effect of chromatic aberration, based on only a single image as input. The technique calculates the defocus effect caused by CA using a sharpening filter, and identifies strong edges (using a difference-of-Gaussian filter) to use for color plane realignment. The technique is evaluated using five 6M pixel images and one 16M pixel image. The execution time (on a 3.2 GHz Pentium 4) for the 6M pixel images was approximately 30 seconds, and for the 16M pixel image 2.5 minutes. In contrast, our technique runs in less than a second for high-resolution images (15M-30M pixels).

Mallon and Whelan [3] present an approach to compensate for chromatic aberration using color plane realignment, similarly to what we do. Their realignment approach is based on image warping. A model of the lateral chromatic aberration over the whole image surface is derived, based on errors from the color filter array. Using partial derivatives of quadratic cost functions, gradients and Hessian matrices are calculated that then are input to the optimization algorithm. They evaluate their approach using three camera models, and only two test images (one chessboard pattern and one outdoor image). A distintive difference in our approach is that it is simpler to calculate using structural instability [16] instead of using derivatives, Hessian matrices, etc.

Zhang *et al.* [17] propose a technique to compensate for lateral CA in a color fringe projection system. A linear compensation model is proposed using phase maps from different color channels to calibrate the magnitude of the lateral CA. The evaluation is done using simulations and three reference images. In contrast, our technique uses a polynomial correction factor.

Chung *et al.* [4] propose a method to detect and eliminate chromatic aberration. They first analyze the color behavior near edges without chromatic aberration and propose a range of limitations for color differences. Pixels violating the color difference range are considered as color fringes. The color channels are then translated separately in horizontal and vertical directions, respectively, using a gradient calculated by horizontal and vertical Sobel gradient. The method is evaluated using 5 images of size 1536×2048, i.e., few and low-resolution images.

Chang *et al.* [6] address the chromatic aberration problem by filtering out false color components from an image, i.e., those components that cause color fringes at edges as a result of chromatic aberration. Their approach relies on adjusting adaptive weights based on color gradients and differences.

Wang *et al.* [1] study the influence of chromatic aberration on demosaicing. They propose a simulation framework for evaluating the influence of CA on demosaicing (one linear interpolation algorithm and one gradient-corrected linear interpolation algorithm). Five images from the Foster set [18] and six images from the CAVE set [19] were used for evaluation. Their most important result is that

correction of chromatic aberration should be done before the demosaicing step.

The approached proposed by Rudakova and Monasse [20] is similar to ours at a high level. They also do sub-pixel alignment of the color planes using high-precision keypoint detection and a radial correction polynomial. However, there are important differences. For example, they identify keypoints based on patterns of black disks on a white background while our approach takes any photo as input and adjusts the correction polynomial based on that particular image. The main disadvantage with their approach is that they only can correct CA in images taken by the same camera-lens combination as the reference image was taken with, while our approach does not require any prior knowledge of the camera-lens combination.

Pi *et al.* [5] present an approach to correct chromatic aberration using a spatially variant total variational model. They employ a spatially variant model to control the gradient matching of the red/blue color channels to the green color channel. They formulate the problem as an optimization problem in order to find the best gradient matching. Their method is very slow, taking approximately 15 seconds on a very low-resolution image of size 310×463 pixels.

An optical approach to correct chromatic aberration is proposed by Wang *et al.* [21]. They designed and fabricated diffractive lenses that could focus the all wavelengths in the visible spectrum onto a single line. However, dispite better lenses, the chromatic aberration problem may exist in images due to, e.g., fabrication errors. Therefore, we strongly believe that blind approaches are necessary as complement to lens-based approaches.

The work by Sun *et al.* [22] is a blind method (just as ours) to correct chromatic aberration. Their approach relies on cross-channel correlation based on pixel-wise similarity. They exploit what they call essential similarity, which is based on the observation that the high-level structures between the color channels are mostly identical. The approach shows good results on both synthetic and real world images. However, the approach is very computational deming, taking 7 seconds to correct a low-resolution 1400×1000 pixels image.

Malleson and Hilton [23] proposes to use a neural network to combine CA correction and demosaicing at the same time. They divide the image into 33 patches and train six convolutional neural networks to account for six 'effective CFA' (color filter array) patterns. Their results show significant improvements in terms of PSNR and SSIM as compared to their baseline approach, which is Matlab's *demosaic* function. However, they do not distinguish between the improvements caused by an improved demosaicing and the improvements caused by the CA correction.

Another approach to simultaneously correct chromatic aberration and do demosaicing is proposed by Llanos [24], [25]. The approach is based on spectral analysis and RGB-to-spectral reconstruction of images. The images are then corrected by estimating aberration-free spectral images.

Correction of chromatic aberration is necessary also in other domains and wavelength spectrum, e.g., in electron microscopy [26]–[29]. In this context, chromatic aberration occurs as electrons that have lost different amounts of energy within an energy window will be focused in different planes by the imaging lens. MacLaren and Ramasse [26] outline how technical advances in the correction of the lens aberrations in the probe-forming lenses have pushed forward atomic-scale structural and chemical characterisation as a result of advances in scanning transmission microscopy. The approach taken in [27] is to do energy-filtered imaging to compensate for the aberration. In [28], [29], the focus is on transmission electron microscopy of liquids and the effects thereof. They show that spatial resolution can be improved by spherical and chromatic aberration correction for liquid samples.

Wang *et al.* [30] propose a chromatic aberration correction approach based on a saturation-value total variation (SVTV) model. The correction is done in the HSV (hue, saturation, value) color space instead of the RGB color space. Gradient matching is done by adjusting the red and blue components to the green components, and intensity is matched between the red, green, and blue components. The solution in their work is set up as an optimization problem that is solved. The approach shows good results in terms of PSNR, SSIM, and SCIELAB error, but is computationally demanding since an optimization problem has to be solved.

Some recent works propose to design lenses that adjust for the different wavelength diffractions [31], [32]. Kim *et al.* [31] use a stack of so called geometric-phase lenses to make sure that the red, green, and blue wavelengths have precisely the same focal length. Zhan *et al.* [32] address the problem of chromatic aberration in immersive virtual reality displays. In their work, they reject digital compensation due to high computation and memory cost. Instead, they propose an optical solution using a hybrid lenses consiting of a combination of Fresnel lenses and Pancharatnam-Berry lenses. Our work shows that the computaional cost can be low when correcting chromatic aberration.

Speed is important in real-time multi-camera stitching. Therefore, Shen *et al.* [33] have proposed a fast chromatic aberration correction technique as part of their stitching solution. Their correction approach is based on averaging the three RGB channels and thus get a mean gray value over an area. Then, each color channel is linearly transformed in relation to the difference to the mean gray value. Their paper does not evaluate the performance of their chromatic aberration correction specifically.

The main properties of our approach that distinguishes it from previous methods are:

- a blind method that only needs one input image, i.e., no lookup tables or prior knowledge of the camera-lens combination,
- the chromatic aberration correction is done on raw bayer data,
- no fixed parameters,

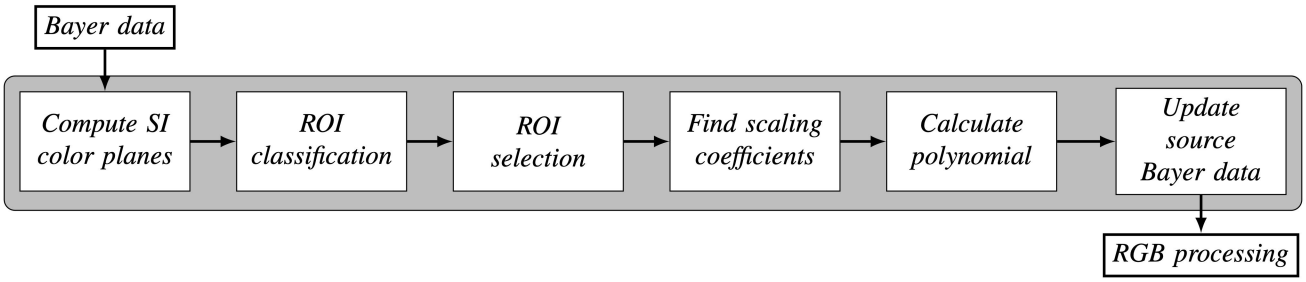

FIGURE 4. Overview of the proposed CA correction method.

- a non-linear re-alignment polynomial, and
- a highly efficient GPU implementation.

III. PROPOSED CORRECTION METHOD

The structural instability (SI) is a simple and efficient metric to identify and assess unstable regions within local Bayer data regions, i.e., regions where the gradient of a color plane is steep. The metric has previously been used to improve interpolation performance of a well known, single computation pass, demosaicing algorithm [16].

Chromatic aberration is a spatial artifact and is therefore easier to analyze and correct in the spatial domain [15]. Previous CA correction methods have been identifying correction parameters by realigning areas where high-contrast edges are present. The problem with most of these methods is that the edges are estimated from RGB color data calculated using linearized, white balanced, demosaiced and color space converted Bayer data. The intense transformation process may have introduced incorrect artifacts that affect the CA correction step.

The SI metric values represent per-pixel instability in the spatial domain and can be seen as a true-edge-map representation of unmodified camera raw Bayer data. Therefore, the per-pixle SI values can be used to realign the color planes of the source Bayer data. In this paper we present a novel SI-based CA-correction method along with a highly efficient GPU-implementation.

Figure 4 shows an overview of our correction method, and Algorithm 1 outlines the major execution steps in the method. In the following sections each step of the correction process is described and motivated. Step 1 is executed once for the entire source Bayer data image. Step 2 is executed once per SI color channel. Steps 3–6 are executed once per red and blue SI color channel. For clarity, *the descriptions of steps 3–6 are in the context of how the red channel is CA corrected* (the blue channel is CA corrected in the same conceptual way). Step 7 is executed once using the CA corrected Bayer data obtained from the previous steps.

A. STEP 1 - COMPUTE THE SI COLOR PLANES

The SI color planes are computed using the theory presented in the original SI paper [16]. For each Bayer location, three corresponding SI values are calculated based on the patterns

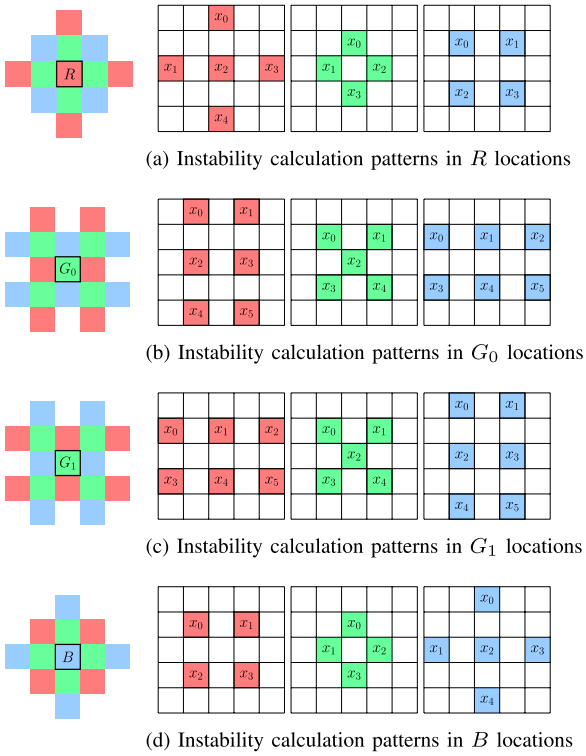

(a) Instability calculation patterns in R locations

(b) Instability calculation patterns in G_0 locations

(c) Instability calculation patterns in G_1 locations

(d) Instability calculation patterns in B locations

FIGURE 5. Predefined pattern sets of local color values used to approximate local structural instability within a color channel [16].

in Figure 5 and as shown in Eq. (1). In this way we get an SI value in each pixel position for each color channel. In essence, calculating the SI values is a very fast approach to calculate an approximation of the gradient of each color plane in each pixel.

$$SI = max\{x_0, \ldots, x_{n-1}\} - min\{x_0, \ldots, x_{n-1}\} \qquad (1)$$

B. STEP 2 - CLASSIFY POTENTIAL REGIONS OF INTEREST (ROI)

The intensity of chromatic aberration increases with the distance from the image center and is more prominent along high-contrast tangential edges. Tangential edges are perpendicular to the radius from the image center, see Figure 6. To be able to identify and classify tangential and radial vectors is a central task in the ROI-selection process. According to [2],

Algorithm 1 Lateral Chromatic Aberration Correction

raw_image ← Raw image data from file
for all *bayer_locations* in *raw_image* **do** ▷ Step 1
  for *color* ← {*red*, *green*, *blue*} **do** ▷ A *bayer_location* is either red, green, or blue
    Calculate SI value according to Figure 5 and Eq. (1)
  end for
end for
Divide *raw_image* into *compute_blocks* of 8 × 8 pixels
for all *compute_blocks* **do** ▷ Step 2
  for *color* ← {*red*, *green*, *blue*} **do**
    top_SI_color ← top *n* SI values in *compute_block*
    mean_top_SI_color ← average of $\forall x \in$ *top_SI_color*
    $\forall x \in$ *top_SI_color* estimate to what extent *x* resides along a radial or tangential edge
  end for
end for
for *color* ← {*red*, *green*, *blue*} **do** ▷ Step 3
  for all *blocks* with value ≥ 0 **do**
    Put *block* in *color_block_list* ▷ One list per color
  end for
end for
for all *top_bayer_locations* from Step 2 in *raw_image* **do** ▷ Step 4
  for *color* ← {*red*, *blue*} **do**
    $CA_{\%} \leftarrow \frac{100 \cdot CA_a}{|\vec{p}-\vec{c}|}$ ▷ CA severity, Eq. (2)
    $ME \leftarrow |\vec{p} - \vec{c}| \cdot \frac{0.3}{100}$ ▷ Maximum extent of CA severity, Eq. (3)
    Calculate a linear scaling factor based on the $CA_{\%}$ from image center
  end for
end for
for *color* ← {*red*, *blue*} **do** ▷ Step 5
  Calculate a polynomial (Eq. (4)) for rescaling the *color* pixels in relation to *green*
end for
for all *bayer_locations* in *raw_image* **do** ▷ Step 6
  for *color* ← {*red*, *blue*} **do**
    Align *color* at *bayer_location* according to the polynomial (Eq. (4))
  end for
end for
for all *bayer_locations* in *raw_image* **do** ▷ Step 7
  Perform RAW to RGB conversion (demosaicing)
end for

CA cannot be measured reliably if the distance from the image center to the measurement position is less than 30% of the distance from the center to the corners. The area (number of pixels) of chromatic aberration in most lenses is roughly proportional to the distance from the image center.

The SI image is conceptually divided into multiple sub-regions of a predefined size. Since the method is intended for GPGPU usage, it is recommended that a computation unit (CU) covers either 8×8 pixels or 16×16 pixels. Each CU is responsible for identifying and calculating the following information:

(i) the top *n* SI values,
(ii) the average of the top *n* SI values, and
(iii) estimate to what extent the top *n* SI values within the block reside along a radial or tangential edge.

The block edge vector is estimated and represented as the line of best fit using the least square method. The per-CU output is: the average of the top *n* SI values scaled by the angle of the estimated edge vector and the pixel coordinates of each of the top *n* SI values. Blocks with high average SI values and edge vectors which are perpendicular to the radius vector from the image center may eventually be processed further in the succeeding steps.

C. STEP 3 - SELECT FINAL REGIONS OF INTEREST

All red and green block results from step 2, with an output value greater than zero, are placed into separate lists which are sorted based on the scaled output value from step 2. It is recommended that multiple sets of lists are defined so that blocks are collected from multiple distances from the

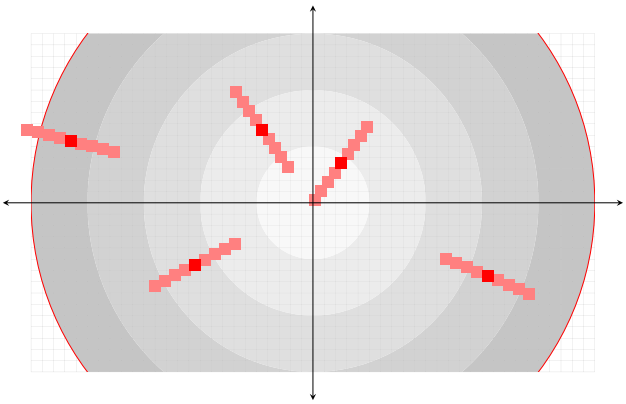

FIGURE 6. Overview of the search area in the proposed CA correction method.

image center. This is important since the polynomial function created in step 5 is relying on scaling factors from multiple image regions with different distances to the image center. In the proposed implementation circular regions are used to ensure that all important spatial locations were covered, see Figure 6. All blocks in each circular region that have the same spatial location and exist in both the red list and the green list are selected for further processing. This means that we select blocks where color gradient is high both in the red and the green color channel. It is recommended to not process all blocks, since the processing time may be significant in images were the number of tangential edges is high.

D. STEP 4 - FIND SCALING COEFFICIENT IN EACH ROI

The goal of this step is to identify a linear scaling factor that re-aligns the red SI color channel to better match the green SI color channel. The linear scaling factor is for that specific distance from the center of the SI image. The blue color channel is re-aligned in exactly the same way. The collection of all linear scaling factors, and their corresponding distances to the SI image center, will later be used to define a polynomial function that is used to correct the chromatic aberration for the entire image.

For each top pixel coordinate from Step 2, one search area is defined. The defined search area consists of multiple sub-pixel coordinates which will be used to sample red and green SI values. The green channel is sampled only once per sub-pixel coordinate and will be used in the structural comparison with the red channel. The red channel is sub-pixel sampled multiple times during the search process.

According to [2], CA can be quantified using the general Eq. (2), which converts CA in pixels (CA_a) to CA as percentage of the distance from the image center to a specific pixel coordinate ($|\vec{p} - \vec{c}|$, where $\vec{p}$ is the pixel location and $\vec{c}$ is the image center). The CA severity is categorized as follows:

- $< 0.04 \Rightarrow$ insignificant
- $0.04 - 0.08 \Rightarrow$ low
- $0.08 - 0.15 \Rightarrow$ moderate
- $> 0.15 \Rightarrow$ strong

In the proposed method, the total search area covers the severity range from 0.00 to 0.30 and its maximum extent (ME), in pixels, is given by Eq. (3). For example, a pixel coordinate with distance of 1000 pixels from image center will have a maximum extent of 3 pixels.

$$CA_{\%} = \frac{100 \cdot CA_a}{|\vec{p} - \vec{c}|} \tag{2}$$

$$ME = |\vec{p} - \vec{c}| \cdot \frac{0.3}{100} \tag{3}$$

In multiple sub-pixel steps, from $-ME * s$ to $ME * s$, the sampling coordinates are re-scaled and used to sample new values from the red color channel of the SI image. In each step, all green values are compared to the current red values. Two scaling factors with the lowest mean-squared-error (MSE) are stored; one factor < 1 and one factor > 1. Scaling factors outside the $-ME$ to ME range are discarded.

E. STEP 5 - CALCULATE POLYNOMIAL

The most common functional approach to model the rescaling factors is a polynomial, see Eq. (4). According to optical theory, the polynomial should only contain even powers [34]. It is common to limit the degree of the polynomial to either six or eight.

$$p(x) = p_n x^n + p_{n-1} x^{n-1} + \ldots + p_2 x^2 + p_1 x + p_0 \tag{4}$$

F. STEP 6 - UPDATE SOURCE BAYER DATA

The most common color filter array (CFA) pattern is the Bayer pattern [7]. In Figure 3 the pattern is illustrated together with the separated color planes, which are used in the proposed technique. The green information is stored in a quincunx grid and the red and blue pixels in rectangular grids.

To CA correct the red channel, the red color values are conceptually concatenated and thereafter sub-pixel resampled. The resampled color intensities are thereafter written back to the source Bayer data, which is then CA corrected. Multiple resampling techniques exist but one recommendation is the Catmull-Rom sampling technique [35]. Our proposed method uses Catmull-Rom for upscaling and uses a linear downscaling. A more thorough evaluation of various sampling techniques for CA correction is left for future work.

G. STEP 7 - RGB PROCESSING

The raw Bayer data is now updated with CA corrected color values for all color channels. Since the data is still unmodified regarding color intensity, black levels, etc. any existing raw Bayer data processing pipeline can be used to generate the final RGB color image representation.

IV. EXPERIMENTAL METHODOLOGY

To evaluate the CA correction performance of our proposed method, we used 25 different raw images. To improve validity, all images are taken by different Canon camera models with no consideration of image content. Three versions of each image were compared; uncorrected, CA corrected

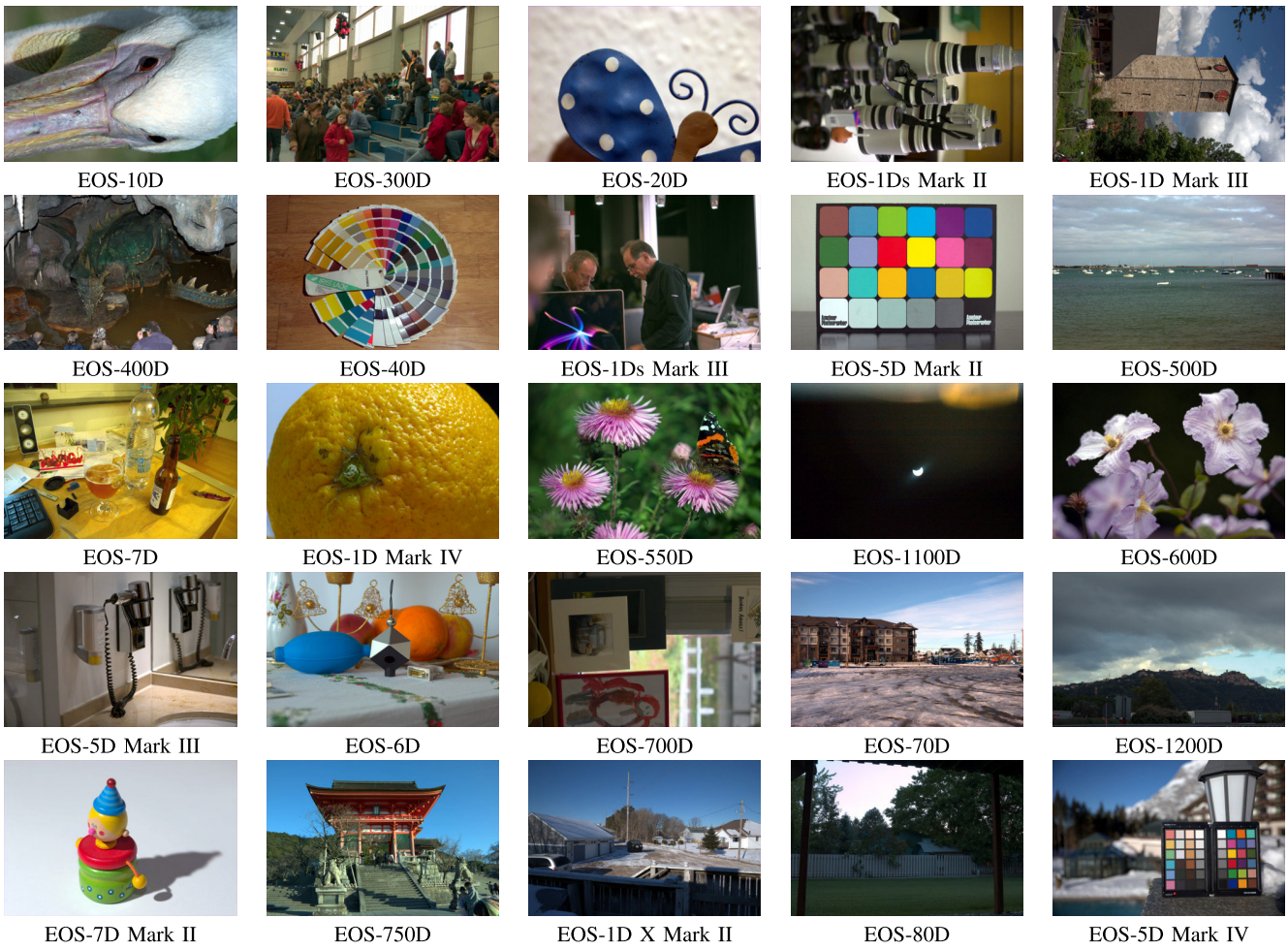

FIGURE 7. The 25 images used when evaluating the CA correction performance of the proposed method.

using DxO Optics Pro, and CA corrected using our proposed method. As evaluation metric we have used variance of the color differences (VCD) [5], [6].

A. TEST IMAGE SET

It is important to select a representative, unbiased, and also diverse set of images for evaluation. In addition, we want to use images freely available to enhance reproducibility and comparability. We have selected 25 images taken with different Canon cameras, and the images are presented in chronological order in Figure 7. All images were downloaded from http://rawsamples.ch/ or https://raw.pixls.us/. The sizes of the images vary from 2048 × 3072 pixels (Canon EOS-10D) to 6720 × 4480 pixels (Canon EOS-5D Mark IV).

More publicly available Canon camera images exist, but were discarded since the DxO Optics Pro software did not support CA correction of those camera combinations. Prior to evaluation, all images were converted to digital negatives (DNG) using the DxO Optics Pro software. All pre- and post-processing features were disabled in the DNG conversion process. The DNG images were then used in all evaluation cases.

B. EVALUATION METRICS

We have selected the variance of the color differences (VCD) as metric for evaluating how well the CA is corrected. The VCD metric has previously been used to evaluate CA artifacts in both almost achromatic images and natural images [5], [6]. We calculate the VCD for the **R**ed channel, VCD_R, and for the **B**lue channel, VCD_B, respectively, see Eq. (5). In Eq. (5), M and N represent the image size, while $Y(i,j)$ and $G(i,j)$ represent the color intensity of the red(R) (or blue(B)) color and the green color, respectively, in the pixel at position (i,j). Lower VCD values represent a lower occurrence of CA artifacts.

$$VCD_Y = \frac{\sum_{i=0}^{M}\sum_{j=0}^{N}[Y(i,j) - G(i,j)]^2}{M \cdot N} \tag{5}$$

C. PARAMETER VARIATION

When evaluating our approach, we have a baseline parameter setting in our algorithm. In the results section, i.e., Section V, we first present results for all images using our default parameter setting, shown in bold in Table 1, i.e., we use a

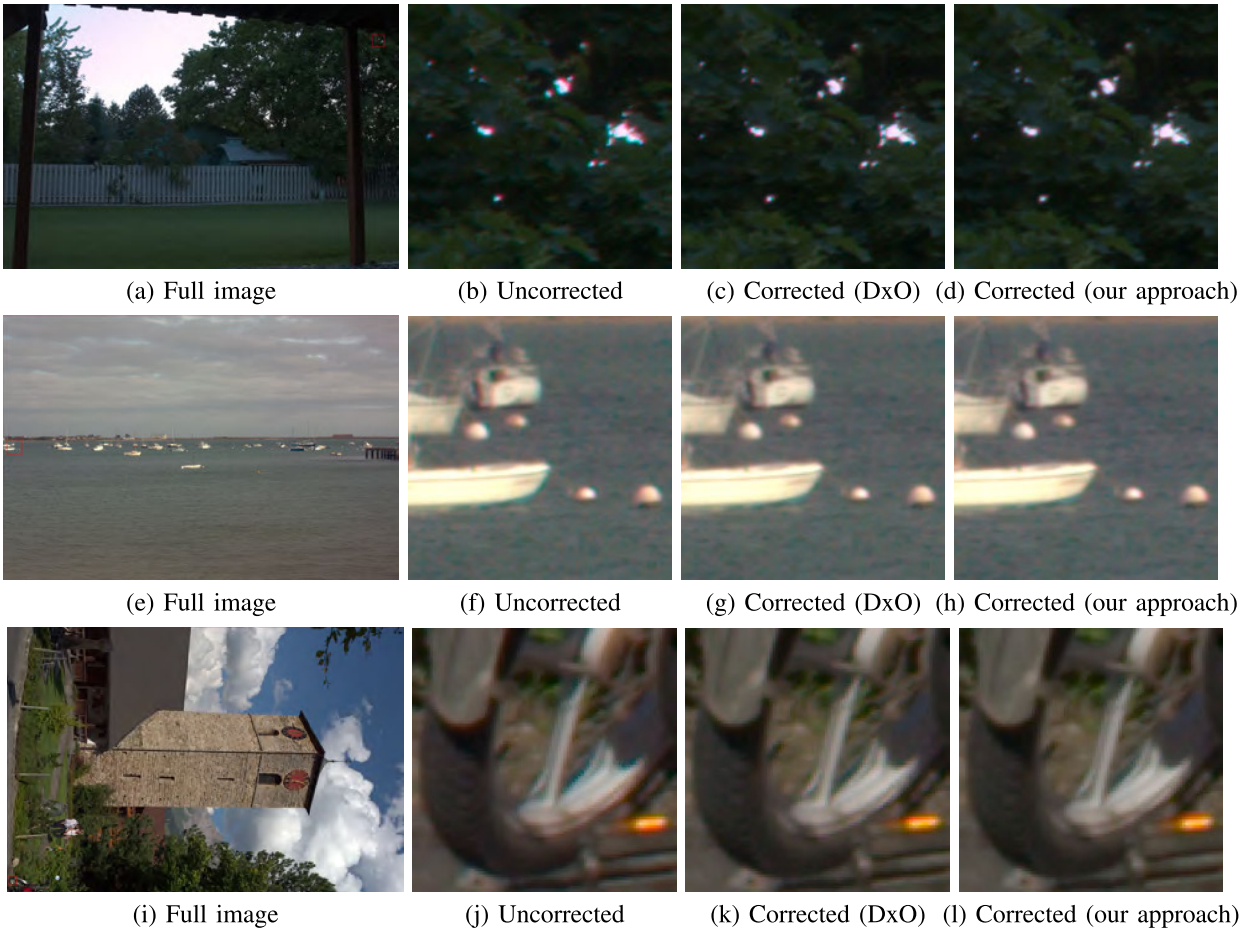

(a) Full image (b) Uncorrected (c) Corrected (DxO) (d) Corrected (our approach)

(e) Full image (f) Uncorrected (g) Corrected (DxO) (h) Corrected (our approach)

(i) Full image (j) Uncorrected (k) Corrected (DxO) (l) Corrected (our approach)

FIGURE 8. Visual comparison of DxO and our correction method, for high resolution ((a)–(d)), medium resolution ((e)–(h)), and low resolution ((i)–(l)) images.

TABLE 1. Parameter variations in the measurements. The default values are marked in bold in the table.

Parameter	Values
Subpixel size	1, **2**, 4
No. of threads	4×4, $\mathbf{8 \times 8}$, 16×16
Number of rings	1, 3, 5, **7**, 9, 11
Demosaicing method	HQLD [10], HQLD_{SI} [16], **DCB** [36], AFD [13], LMMSE [8]

subpixel size of 2, 8×8 threads, 7 rings, and DCB [36] for demosaicing.

In order to evaluate the impact of different parameter settings, we have varied one parameter at a time, as shown in Table 1, while the other parameters keep their default values. The used demosaicing methods represent a wide range of methods where computational complexity and interpolation quality vary. In the results section we present the average results, for each parameter setting, for all images.

V. EXPERIMENTAL RESULTS AND ANALYSIS

We start our analysis with looking at the results with the default parameters for our algorithm in Section V-A. Then, we evaluate how the CA corrrection capability of our algorithm are affected for different parameter settings in Section V-B.

A. CA CORRECTION RESULTS

In Table 2, we present the VCD values for each of the images. We present values for uncorrected (Raw) images, images CA corrected using DxO Optics Pro, and images CA corrected using our method with default parameters. Numbers in bold indicate the best alternative for that particular image for each of the red and blue color channels (green is the reference color and is unchanged).

We start by looking at the bottom line in Table 2, where the average VCD values over all images are presented. We observe that our proposed method is better at correcting chromatic aberration than DxO Optics Pro, averaged over 25 images, for both the red and the blue color channel.

Looking at the results for individual images, we observe that our proposed method is best in 14 cases for the red color and 14 cases for the blue color, while DxO Optics Pro is best in 8 cases for the red color and 10 cases for the blue color. Thus, our proposed method is better in general, despite the lack of prior knowledge of the camera-lens combination.

TABLE 2. Comparison of VCD values when demosaicing using DCB and 7 rings, 64 samples per search vector and 2 sample locations per pixel.

	Camera model	Resolution (MP)	Uncorrected Raw		Corrected using DxO		Proposed Method	
			VCD_R	VCD_B	VCD_R	VCD_B	VCD_R	VCD_B
01	EOS-10D	6.29	34.32	**19.62**	34.32	**19.62**	**34.28**	19.63
02	EOS-300D	6.29	493.18	287.59	494.30	287.34	**491.82**	**282.89**
03	EOS-20D	8.19	255.26	98.69	254.99	98.56	**254.83**	**98.55**
04	EOS-1Ds Mark II	16.61	**305.84**	144.62	305.86	144.58	305.87	**144.53**
05	EOS-1D Mark III	10.08	38.30	58.45	38.15	58.50	**37.89**	**58.44**
06	EOS-400D	10.08	53.46	31.90	**51.04**	**30.48**	51.50	30.97
07	EOS-40D	10.08	152.48	114.42	**152.41**	114.19	152.48	**114.13**
08	EOS-1Ds Mark III	21.03	472.74	312.57	**472.66**	312.14	472.77	**310.41**
09	EOS-5D Mark II	21.03	165.18	155.25	163.37	154.28	**158.20**	**152.19**
10	EOS-500D	15.05	10.48	29.95	10.22	29.92	**10.14**	**29.87**
11	EOS-7D	17.92	1166.22	**147.56**	1166.89	148.28	**1164.88**	147.57
12	EOS-1D Mark IV	15.98	**1707.44**	280.85	1707.73	280.91	1708.61	**280.79**
13	EOS-550D	17.92	508.49	193.41	509.15	**193.37**	**508.16**	193.39
14	EOS-1100D	12.17	**0.15**	**0.09**	**0.15**	**0.09**	**0.15**	**0.09**
15	EOS-600D	17.92	3.83	11.84	3.81	**11.82**	**3.76**	**11.82**
16	EOS-5D Mark III	22.12	375.18	154.68	374.87	**153.99**	**374.71**	154.20
17	EOS-6D	20.65	524.72	450.68	**524.18**	**448.95**	524.41	449.93
18	EOS-700D	17.92	146.49	**457.04**	145.76	457.12	**145.58**	**457.04**
19	EOS-70D	20.65	126.94	217.55	**125.88**	**214.67**	126.19	214.95
20	EOS-1200D	17.92	47.82	34.44	47.89	34.29	**47.79**	**34.27**
21	EOS-7D Mark II	20.65	73.48	38.24	73.29	**38.09**	**72.99**	38.11
22	EOS-750D	24.73	483.33	740.74	**458.48**	**738.50**	459.38	739.10
23	EOS-1D X Mark II	20.65	97.95	196.69	**94.21**	**196.61**	94.42	196.71
24	EOS-80D	25.5	156.67	163.96	112.08	163.52	**106.07**	**161.28**
25	EOS-5D Mark IV	31.26	56.09	60.15	**56.07**	60.12	56.10	**60.11**
Avg:		15.29	298.24	176.04	295.11	175.60	**294.52**	**175.24**

TABLE 3. Results showing how different CA correction parameters affect the VCD values in the red and blue color channels.

Demosaicing	Rings	Samples	Subpixels	Raw_{VCD_R}	Raw_{VCD_B}	DxO_{VCD_R}	DxO_{VCD_B}	$Proposed_{VCD_R}$	$Proposed_{VCD_B}$
AFD	7	8×8	2	295.12	174.30	292.32	173.90	292.38	173.74
DCB	7	8×8	2	298.24	176.04	295.11	175.60	294.52	175.24
HQLD	7	8×8	2	296.89	175.08	293.71	174.64	293.62	174.41
$HQLD_{SI}$	7	8×8	2	297.27	175.35	294.10	174.91	294.02	174.63
LMMSE	7	8×8	2	291.40	172.78	289.81	172.54	289.80	172.36
				295.17	174.37	292.48	174.00	**292.45**	**173.79**
DCB	1	8×8	2	298.24	176.04	295.11	175.60	295.33	175.52
DCB	3	8×8	2	298.24	176.04	295.11	175.60	294.55	175.26
DCB	5	8×8	2	298.24	176.04	295.11	175.60	294.52	175.24
DCB	7	8×8	2	298.24	176.04	295.11	175.60	294.52	175.24
DCB	9	8×8	2	298.24	176.04	295.11	175.60	294.50	175.23
DCB	11	8×8	2	298.24	176.04	295.11	175.60	294.49	175.23
				298.24	176.04	295.11	175.60	**294.68**	**175.29**
DCB	7	4×4	2	298.24	176.04	295.11	175.60	294.58	175.23
DCB	7	8×8	2	298.24	176.04	295.11	175.60	294.52	175.24
DCB	7	16×16	2	298.24	176.04	295.11	175.60	294.79	175.40
				298.24	176.04	295.11	175.60	**294.68**	**175.31**
DCB	7	8×8	1	298.24	176.04	295.11	175.60	294.58	175.28
DCB	7	8×8	2	298.24	176.04	295.11	175.60	294.52	175.24
DCB	7	8×8	4	298.24	176.04	295.11	175.60	294.46	175.18
DCB	7	8×8	8	298.24	176.04	295.11	175.60	294.57	175.22
				298.24	176.04	295.11	175.60	**294.53**	**175.22**

Based on the numbers in Table 2 it is difficult to make any general conclusion of when DxO Optics Pro is better or when our method is better, e.g., in terms of image content, resolution, etc. Surprisingly, we found that in some rare cases

both DxO Optics Pro as well as our method degrade the image quality in terms of chromatic aberration.

In Figure 8, we show some visual comparison between the uncorrected image and the versions corrected using DxO Optics Pro and our method, respectively. We have selected representative images of high resolution (top row), medium resolution (middle row), and low resolution (bottom row). In general, there is virtually no visual difference between the corrected images, i.e., both DxO Optics Pro and our method manage to remove or reduce the color fringes present in the uncorrected image.

B. PARAMETER VARIATION

In order to evaluate how stable our method is, we varied a number of parameters for the algorithm, i.e., the number of rings, the number of subpixels, the sample size, and the demosaic method, as listed in Table 1. When varying one parameter, all other parameters were fixed to the default values (a subpixel size of 2, 8 × 8 threads, 7 rings, and DCB for demosaicing). All 25 test images were CA corrected using varying correction parameters.

The correction results, averaged over all 25 test images, using varying parameters are presented in Table 3. No major differences were observed when altering the ring count, the sample count, or the subpixel count. Instead, the most notably effect was observed when altering the demosaicing method used. Further, in line with results in Section V-A, our method are in general better than DxO Optics Pro in correcting chromatic aberration.

VI. CONCLUSION

Chromatic aberration is a problem in color images as a result of different refraction angels in lenses for light of different wavelengths. As a result, red or blue fringes may show up around edges and in high contrast areas of the image. Contemporary solutions mostly rely on lookup tables with unique correction parameters for each camera/lens combination.

In this paper, we propose a blind method to correct chromatic aberration errors in color images. We call our method blind since it *does not rely on any prior knowledge* of how the image was captured, i.e., it requires no information about the camera/lens combination or any correction parameters.

The method (i) dynamically identifies the regions in the image that have the largest structural instability (steepest changes in the different color planes), (ii) calculates a correction polynomial based on computed scaling coefficients, and (iii) finally aligns the different color planes according to the correction polynomial.

We evaluate our method in comparison to DxO Optics Pro using 25 test images and the variance of the color differences (VCD) metric. The results show that our blind method has a similar or slightly better error correction performance as DxO Optics Pro, but without prior knowledge of the camera-lens setup.

IMAGE CREDITS

All test images were taken from http://rawsamples.ch/ or https://raw.pixls.us/, and they all have the Creative Common License CC0 or CC-BY-NC-SA.

REFERENCES

[1] X. Wang, M. Pedersen, and J. Thomas, "The influence of chromatic aberration on demosaicking," in *Proc. 5th Eur. Workshop Vis. Inf. Process. (EUVIP 2014)*, Dec. 2014, pp. 1–6.

[2] Imatest. (2017). *Chomatic Aberration AKA Color Fringing*. Accessed: Apr. 5, 2017. [Online]. Available: http://www.imatest.com/docs/sfr_chromatic/

[3] J. Mallon and P. F. Whelan, "Calibration and removal of lateral chromatic aberration in images," *Pattern Recognit. Lett.*, vol. 28, no. 1, pp. 125–135, 2007.

[4] S.-W. Chung, "Removing chromatic aberration by digital image processing," *Opt. Eng.*, vol. 49, no. 6, Jun. 2010, Art. no. 067002.

[5] L. Pi, W. Wang, and M. Ng, "A spatially variant total variational model for chromatic aberration correction," *J. Vis. Commun. Image Represent.*, vol. 41, pp. 296–304, Nov. 2016.

[6] J. Chang, H. Kang, and M. G. Kang, "Correction of axial and lateral chromatic aberration with false color filtering," *IEEE Trans. Image Process.*, vol. 22, no. 3, pp. 1186–1198, Mar. 2013.

[7] B. Bayer, "Color imaging array," U.S. Patent 3 971 065, Jul. 20, 1976. [Online]. Available: http://www.google.com/patents/US3971065

[8] D. Zhang and X. Wu, "Color demosaicking via directional linear minimum mean square-error estimation," *IEEE Trans. Image Process.*, vol. 14, no. 12, pp. 2167–2178, Dec. 2005.

[9] X. Wu and N. Zhang, "Primary-consistent soft-decision color demosaicking for digital cameras (patent pending)," *IEEE Trans. Image Process.*, vol. 13, no. 9, pp. 1263–1274, Sep. 2004.

[10] H. S. Malvar, L.-w. He, and R. Cutler, "High-quality linear interpolation for demosaicing of Bayer-patterned color images," in *Proc. IEEE Int. Conf. Acoust., Speech, Signal Process.*, May 2004, p. 485.

[11] K.-H. Chung and Y.-H. Chan, "Color demosaicing using variance of color differences," *IEEE Trans. Image Process.*, vol. 15, no. 10, pp. 2944–2955, Oct. 2006.

[12] B. K. Gunturk, Y. Altunbasak, and R. M. Mersereau, "Color plane interpolation using alternating projections," *IEEE Trans. Image Process.*, vol. 11, no. 9, pp. 997–1013, Sep. 2002.

[13] N.-X. Lian, L. Chang, Y.-P. Tan, and V. Zagorodnov, "Adaptive filtering for color filter array demosaicking," *IEEE Trans. Image Process.*, vol. 16, no. 10, pp. 2515–2525, Oct. 2007.

[14] J. Kühn, T. Colomb, F. Montfort, F. Charrière, Y. Emery, E. Cuche, P. Marquet, and C. Depeursinge, "Real-time dual-wavelength digital holographic microscopy with a single hologram acquisition," *Opt. Exp.*, vol. 15, no. 12, pp. 7231–7242, Jun. 2007.

[15] S. B. Kang, "Automatic removal of chromatic aberration from a single image," in *Proc. IEEE Conf. Comput. Vis. Pattern Recognit. (CVPR)*, Jun. 2007, pp. 1–8.

[16] S. Petersson, H. Grahn, and J. Rasmusson, "Color demosaicing using structural instability," in *Proc. IEEE Int. Symp. Multimedia (ISM)*, Dec. 2016, pp. 541–544.

[17] Z. H. Zhang, C. E. Towers, and D. P. Towers, "Compensating lateral chromatic aberration of a colour fringe projection system for shape metrology," *Opt. Lasers Eng.*, vol. 48, no. 2, pp. 159–165, Feb. 2010.

[18] D. H. Foster, K. Amano, S. M. C. Nascimento, and M. Foster, "Frequency of metamerism in natural scenes," *J. Opt. Soc. Amer. A, Opt. Image Sci.*, vol. 23, no. 12, pp. 2359–2372, 2006.

[19] F. Yasuma, T. Mitsunaga, D. Iso, and S. K. Nayar, "Generalized assorted pixel camera: Postcapture control of resolution, dynamic range and spectrum," Dept. Comput. Sci., Columbia Univ., New York, NY, USA, Tech. Rep. CUCS-061-08, Nov. 2008. [Online]. Available: http://wwwl.cs.columbia.edu/CAVE/ databases/multispectral/

[20] V. Rudakova and P. Monasse, "Precise correction of lateral chromatic aberration in images," in *Image and Video Technology*, R. Klette, M. Rivera, and S. Satoh, Eds. Berlin, Germany: Springer, 2014, pp. 12–22.

[21] P. Wang, N. Mohammad, and R. Menon, "Chromatic-aberration-corrected diffractive lenses for ultra-broadband focusing," *Sci. Rep.*, vol. 6, no. 1, pp. 1–7, Aug. 2016.

[22] T. Sun, Y. Peng, and W. Heidrich, "Revisiting cross-channel information transfer for chromatic aberration correction," in *Proc. IEEE Int. Conf. Comput. Vis. (ICCV)*, Oct. 2017, pp. 3248–3256.
[23] C. Malleson and A. Hilton, "Joint demosaicing and chromatic aberration correction of images using neural networks," in *Proc. Conf. Vis. Media Prod.*, Nov. 2019, p. 1.
[24] B. Llanos, "Chromatic aberration correction and spectral reconstruction from colour images," M.S. thesis, Dept. Comput. Sci., Univ. Alberta, Edmonton, AB, Canada, 2019.
[25] B. Llanos and Y.-H. Yang, "Simultaneous demosaicing and chromatic aberration correction through spectral reconstruction," in *Proc. 17th Conf. Comput. Robot Vis. (CRV)*, May 2020, pp. 17–24.
[26] I. MacLaren and Q. M. Ramasse, "Aberration-corrected scanning transmission electron microscopy for atomic-resolution studies of functional oxides," *Int. Mater. Rev.*, vol. 59, no. 3, pp. 115–131, Apr. 2014.
[27] F. F. Krause, A. Rosenauer, J. Barthel, J. Mayer, K. Urban, R. E. Dunin-Borkowski, H. G. Brown, B. D. Forbes, and L. J. Allen, "Atomic resolution elemental mapping using energy-filtered imaging scanning transmission electron microscopy with chromatic aberration correction," *Ultramicroscopy*, vol. 181, pp. 173–177, Oct. 2017.
[28] N. de Jonge, "Theory of the spatial resolution of (scanning) transmission electron microscopy in liquid water or ice layers," *Ultramicroscopy*, vol. 187, pp. 113–125, Apr. 2018.
[29] N. de Jonge, L. Houben, R. E. Dunin-Borkowski, and F. M. Ross, "Resolution and aberration correction in liquid cell transmission electron microscopy," *Nature Rev. Mater.*, vol. 4, no. 1, pp. 61–78, Jan. 2019.
[30] W. Wang, L. Pi, and M. K. Ng, "Saturation-value total variation model for chromatic aberration correction," *Inverse Problems Imag.*, vol. 14, no. 4, pp. 733–755, 2020.
[31] J. Kim, K. J. Hornburg, M. J. Escuti, and N. Z. Warriner, "Chromatic-aberration correction in geometric-phase lenses, for red, green, and blue operation (conference presentation)," *Proc. SPIE*, vol. 10361, Sep. 2017, Art. no. 1036113.
[32] T. Zhan, J. Zou, J. Xiong, X. Liu, H. Chen, J. Yang, S. Liu, Y. Dong, and S. Wu, "Practical chromatic aberration correction in virtual reality displays enabled by cost-effective ultra-broadband liquid crystal polymer lenses," *Adv. Opt. Mater.*, vol. 8, no. 2, Jan. 2020, Art. no. 1901360.
[33] J. Shen, F. Qian, and X. Chen, "Multi-camera panoramic stitching with real-time chromatic aberration correction," *J. Phys., Conf. Ser.*, vol. 1617, Aug. 2020, Art. no. 012046.
[34] W. Hugemann, *Correcting Lens Distortions in Digital Photographs*. Brussels, Belgium: EVU, 2010.
[35] J. Li, Y. Koudota, M. Barkowsky, H. Primon, and P. L. Callet, "Comparing upscaling algorithms from HD to Ultra HD by evaluating preference of experience," in *Proc. 6th Int. Workshop Qual. Multimedia Exper. (QoMEX)*, Sep. 2014, pp. 208–213.
[36] J. Gozdz. (2010). *DCB Demosaicing Algorithm*. [Online]. Available: http://www.linuxphoto.org/html/dcb.html

STEFAN PETERSSON received the B.Sc. and M.Sc. degrees in computer science from the Blekinge Institute of Technology (BTH), where he is currently pursuing Ph.D. degree within the BigData@BTH Project. He has been a Lecturer with BTH, since 2007. From 2011 to 2019, he was a Program Manager of the master of science with the Game and Software Engineering Program, BTH. He is currently a Research Engineer within the BigData@BTH Project. His current interests include computer graphics, image processing, and GPGPU.

HÅKAN GRAHN received the M.Sc. degree in computer science and engineering and the Ph.D. degree in computer engineering from Lund University, in 1990 and 1995, respectively. From January 1999 to June 2002, he was the Head of the Department of Software Engineering and Computer Science. From 2011 to 2013, he was the Dean of research with the Blekinge Institute of Technology. He is currently a Professor of computer engineering with the Department of Computer Science, Blekinge Institute of Technology. He lead the research project "Scalable resource-efficient system for big data analytics," funded with 36 MSEK by the Knowledge Foundation, from 2014 to 2020. He has published more than 100 articles on these subjects, including 25 journal articles. His main interests include computer architecture, multicore systems, parallel computing, performance evaluation, image processing, and AI/machine learning.

JIM RASMUSSON received the M.Sc. and Tech. Lic. degrees from Lund University. Since 1990, he has been working in the mobile phone industry. He has a long history of multimedia oriented algorithms and processing, including camera, image, graphics, computer vision, machine learning, speech, and audio. Recent main focus is visual media machine learning on heterogeneous processing systems.